

Effect of Zirconium Substitution on Structural, Dielectric and Electrical Properties of Lead-free $\text{Li}_{0.5}\text{Bi}_{0.5}\text{Ti}_{0.9}\text{Zr}_{0.1}\text{O}_3$ Ceramics

D. Panda¹, B. B. Mohanty², P. S. Sahoo³, R. N. P. Choudhary⁴

¹Technical Officer-B, Department of Imaging Wing, PXE, DRDO, Balasore, India

²Lecturer, Department of Physics, Betnoti College, Betnoti, India

³Reader, Department of Physics, North Orissa University, Baripada, India

⁴Professor, Department of Physics, ITER, Bhubaneswar, India

Abstract: Ceramic samples of Zirconium substituted Lithium Bismuth Barium Titanate of composition $\text{Li}_{0.5}\text{Bi}_{0.5}\text{Ti}_{0.9}\text{Zr}_{0.1}\text{O}_3$ a polycrystalline orthorhombic compound have been synthesized by conventional solid state reaction method at high temperature (i.e., at 900°C).

The effect of Zr (0.1) on the structural and microstructural properties of $\text{Li}_{0.5}\text{Bi}_{0.5}\text{Ti}_{0.9}\text{Zr}_{0.1}\text{O}_3$ was investigated by XRD and SEM. The room temperature X-ray diffraction study assured the evolution of single-phase compound with orthorhombic structure. The dielectric analysis of $\text{Li}_{0.5}\text{Bi}_{0.5}\text{Ti}_{0.9}\text{Zr}_{0.1}\text{O}_3$ explored over a broad frequency range ($10^3 - 10^6$ Hz) at various temperatures (33°C-500°C) displayed that the dielectric properties of the material are dependent on both frequency and temperature. Dielectric study reveals that the ferro to paraelectric phase transition of the studied compound is a temperature of 257°C. The nature of the variation of conductivity and value of activation energy in different regions, calculated from the temperature dependence of ac conductivity suggest that the conduction process is of mixed type (i.e., ionic-polaronic and space charge generated from the oxygen ion vacancies). AC impedance plots as a function of frequency at different temperatures were used to analyse the electrical behaviour of the sample, which indicated the negative temperature coefficient of resistance character. Complex impedance analysis targeted the relaxation phenomenon is poly disperse and non-Debye type in nature.

Keywords: Ceramics, Perovskite structure, Solid-state reaction, X-Ray Diffraction, dielectric, Impedance, Dielectric relaxation.

1. Introduction

Since the revelation of barium titanate, BaTiO_3 , in polycrystalline structure, it has been broadly utilized in different electronic segments, for example, multilayer capacitor (MLCs), positive temperature coefficients of resistivity (PTCR) thermistor, piezoelectric gadget, optoelectronic segments and semiconductors (Morrison et al 2001; Weber et al 2001; Mahajan et al 2009). Valuable properties for business gadget applications have been generally watched initially in toxic perovskite mixes, for example, PMN-PT, PNN-PZT, PLZT and PZT (Park and Shrout 1997; Fu and Cohen 2000; Mahajan et al 2009). These pieces have a conspicuous detriment of

unpredictability and harmfulness of 'lead'. Reckoning the above, the ferroelectric oxides of perovskite structural family have chiefly been probed for their convenient dielectric [4], electro-optic [5], nonlinear optic [6] pyroelectric [7], piezoelectric [5] properties. The increasing demand for environmentally benign materials in the electronics industry is now focused on lead free ceramics comparable to lead-based ceramics for solid state device applications. (1-3) Perovskite structure materials with the general formula ABO_3 (where, A = mono or divalent cations and B = tri, tetra, penta, or hexavalent cations) are found to be very useful for different solid state devices. The A particles involve the edges of the 3D square, which is 12 composed, while the B particles sit on the body focus positions inside an oxygen octahedron, which are at the face focus positions. Literature survey disclosed that an abundant of research has been cultivated on perovskite type ferroelectric oxides niobates and tantalates [11]-[13]. We couldn't discover any, however, no work is executed on the auxiliary, dielectric and electrical properties of current compound. Looking to the significance of the material, we have combined and investigated the auxiliary and dielectric properties of another compound having the concoction equation $\text{Li}_{0.5}\text{Bi}_{0.5}\text{Ti}_{0.9}\text{Zr}_{0.1}\text{O}_3$.

2. Experimental Procedure

A. Material preparation

The stoichiometric ratio of starting chemicals LiCO_3 (>99.9%), Bi_2O_3 (>99.9%), TiO_2 (>99.9%) and ZrO_2 (>99.9%) were weighed for the composition $\text{Li}_{0.5}\text{Bi}_{0.5}\text{Ti}_{1-x}\text{Zr}_x\text{O}_3$ ($x = 0.1$). The weighed powders were blended mechanically by an agate mortar for about 3 h. The powders were then calcined at optimized temperature and time (900°C for 12 h) in air condition. The calcined powder thus procured was blended with PVA (poly vinyl alcohol) binder, grinded and were palletized ensuingly (about 10 mm in diameter and 1 - 2 mm thickness) under uniaxial pressure of 4×10^6 N/m². Thereafter the pellets were sintered in air atmosphere at 950°C

for 12 h. Ultimately the pellets were laminated with high purity silver paint, and then heated at 150°C for 2 h before executing the electrical measurements.

B. Material characterisation

X-ray diffraction (XRD) pattern of the material procured in a vast range of Bragg angle 2θ ($20^\circ \leq 2\theta \leq 80^\circ$) at a scanning speed of $3^\circ/\text{min}$ by an X-ray diffractometer (Rigaku, Miniflex) with $\text{CuK}\alpha$ radiation ($\lambda = 1.5405 \text{ \AA}$) at room temperature. The surface morphology of the pellet sample of the material was recorded with a high-resolution scanning electron microscope (SEM: JOEL-JSM model: 5800F). The dielectric characterisation of the sample was prosecuted in the temperature range of $32^\circ\text{C} - 5000^\circ\text{C}$ and frequency range of 1 kHz to 1 MHz, using a computer-controlled Hioki HiTester LCR meter.

3. Results and Discussion

A. Structural and microstructural analysis

Figure 1 and 2 shows the XRD pattern of the sample. Ordering of all the peaks of the pattern were done taking their 2θ values by a computer program package, "POWDMULT" [14] in distinct crystal system and cell configuration and are traced to be sharp and solo, which The peaks are discrete from those of ingredients ensuring the evolution of new single-phase compound. On the basis of the best agreement (based on least-squares refinement) between scrutinised (obs) and reckoned (cal) inter planer distance d (i.e., $\sum (\text{dobs} - \text{dcal}) = \text{minimum}$), an orthorhombic unit cell was selected with lattice parameters: $a = 14.0644 (29) \text{ \AA}$, $b = 4.2402 (29) \text{ \AA}$, $c = 17.4749 (29) \text{ \AA}$ (estimated standard deviation in parentheses) which are consistency with the reported ones [15].

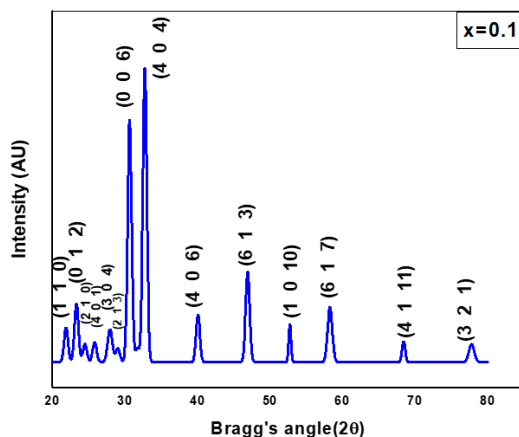


Fig. 1. Room temperature XRD pattern of $\text{Li}_{0.5}\text{Bi}_{0.5}\text{Ti}_{0.9}\text{Zr}_{0.1}\text{O}_3$ compound

The coherently average dispersed crystallite size (D) of the compound was computed to be $\sim 15 \text{ nm}$ using Scherrer's equation; $D = 0.89\lambda/(\beta/2\cos\theta hkl)$, where $\lambda = 1.5405 \text{ \AA}$ and $\beta/2 = \text{peak width of the reflection at half maxima}$ [16]. The contributions of strain, instrumental error and other unknown effects in the peak broadening have not been taken into board

during the crystallite size enumeration. The room temperature SEM micrograph (Figure 2 (left)) of the LBTZ compound, confirmed homogenously and non-uniform distribution of the grains over the entire surface of the sample. The grain size evaluated from the histogram Figure 2 (right) is traced to be of $9.6 \mu\text{m}$. As expected, the grain size of the sample obtained here is gigantic in comparison to the crystallite size enumerated from Scherrer's equation. Thus, a solo grain has large number of crystallites [17].

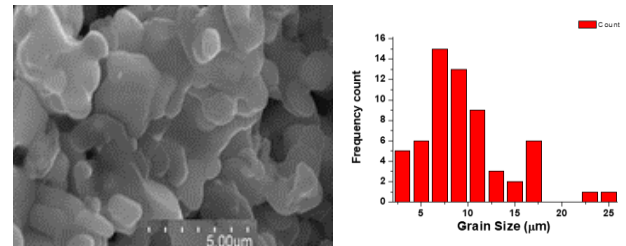


Fig. 2. SEM micrographs and histogram (left) and histogram (right) of $\text{Li}_{0.5}\text{Bi}_{0.5}\text{Ti}_{0.9}\text{Zr}_{0.1}\text{O}_3$ compound

B. Dielectric Analysis

The variation of dielectric parameters (relative dielectric permittivity (ϵ_r) and loss tangent ($\tan\delta$)) with frequency is shown in Fig.3. Both dielectric permittivity (ϵ_r) and loss ($\tan\delta$) decrease sharply with the rise in frequency which is a general property of dielectric materials [4], [5]. The value of dielectric constant decreases at higher frequencies, and eventually reaches a constant value that may be due to the slower movement/hopping of electrons in dielectric materials [22]. The electron hopping at high frequency cannot follow the changing electric field hence they have to move through grain and grain boundaries. Since the grain boundaries have high resistance it causes space charge polarisation as the electrons pileup there which increases dielectric constant at a lower frequency. At higher frequency dielectric constant declines as the accumulation of charges at grain boundaries decreases. The Maxwell-Wagner and Koop's phenomenological models explain such type of dielectric behaviour (i.e., in the region of lower frequency the dielectric constant declines quickly while at higher frequency region it declines slowly) [23]. Based on these models, the structure of the dielectric material is divided into two layers (i.e., the highly conducting grains effective at high frequency and poorly conducting grain boundaries effective at lower frequencies). The tangent loss ($\tan\delta$) varies in a similar fashion, as in that of ϵ_r with frequency. The $\tan \delta$ is usually higher in the lower frequency region due to higher resistance of grain boundaries for which more energy is needed for the movement of electrons. In the higher region of frequency, the resistance is low which indicates lower value of $\tan\delta$. This may be due to the dielectric relaxation phenomena occurring in the compound [24].

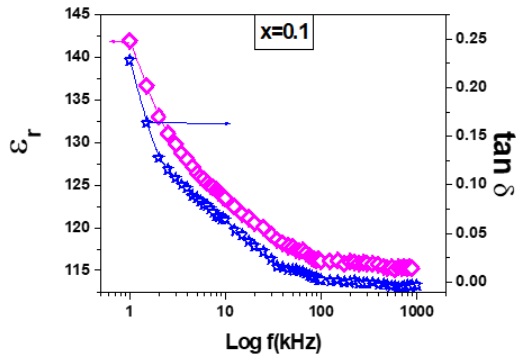


Fig. 3. $\epsilon_r \sim \log f$ & $\tan \delta \sim \log f$ graphs of $\text{Li}_{0.5}\text{Bi}_{0.5}\text{Ti}_{0.9}\text{Zr}_{0.1}\text{O}_3$ at room temperatures

The temperature variety of relative dielectric constant ϵ_r at some chosen frequencies of compound is demonstrated in Figure 4. It can be observed that in the low- and medium-temperature ranges, the value of dielectric constant is nearly constant, and then on a further rise in temperature, it increases slowly. This trend of increase in relative dielectric constant may be due to the motion of space charges [26]. The plot solidly settled the ferro to paraelectric stage progress at 258°C . The estimation of ϵ_r is small at low temperatures which increments with an increase in temperature. The dielectric constant (ϵ_r) at frequencies 10, 50, 100, 500 and 1000 kHz are seen as 145, 130, 108, 90 and 87 respectively at the transition temperature. The variety of $\tan \delta$ follows a similar pattern as that of ϵ_r . The expansion in the estimation of $\tan \delta$ might be expected to (i) improvement in the conductivity and (ii) decrease in the commitment of ferroelectric domain wall [18].

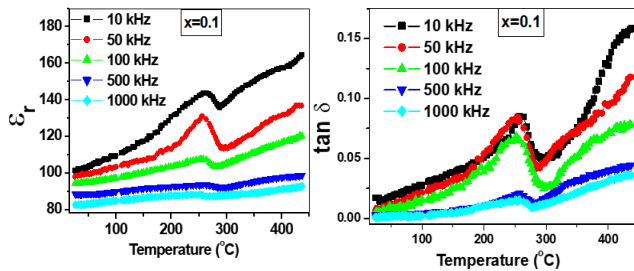


Fig. 4. Variation of ϵ_r and $\tan \delta$ (right) with temperature of $\text{Li}_{0.5}\text{Bi}_{0.5}\text{Ti}_{0.9}\text{Zr}_{0.1}\text{O}_3$ at some selected frequencies

C. AC Conductivity Analysis

The ac electrical conductivity (σ_{ac}) is determined utilizing the dielectric information and an empirical connection. $\sigma_{ac} = \omega \epsilon_r \epsilon_0 \tan \delta$, where ϵ_0 = permittivity of free space and ω = angular frequency. Figure 5 shows the variation of σ_{ac} as a function of temperature at frequencies 10 and 100 kHz. The nature of the variation (Figure 5) is almost linear over a wide temperature area complying with the Arrhenius relation: $\sigma_{ac} = \sigma_0 \exp(-E_a/k_B T)$ [19], each of the charts is divided into two unique regions independently of frequency. Every divided region is characterized by different slopes showing different

activation energy. The solid line of figure shows the linear fit. The activation energy calculated from the slope of the curve at different temperatures has been compared in Table 1. Because of the dielectric phase transitions, abnormality in conductivity was observed for the entire compound at temperatures nearly equal to its Curie temperature, which may be because of the dielectric phase transitions. The value of σ_{ac} increases with an increase in temperature indicating negative temperature coefficient of resistance (NTCR) behavior. The increase in conductivity is due to the hopping action of the ions because of thermally activated electrons. At high temperature higher value of activation energy indicates that conductivity is for the movement of oxygen vacancies. Activation energy is low at high frequency as compared to that at the low frequency (Table 1). This is because at low frequencies the overall conductivity is the result of hopping of charge carriers over a large distance and at higher frequencies is restricted to only nearest neighbouring defects sites [20].

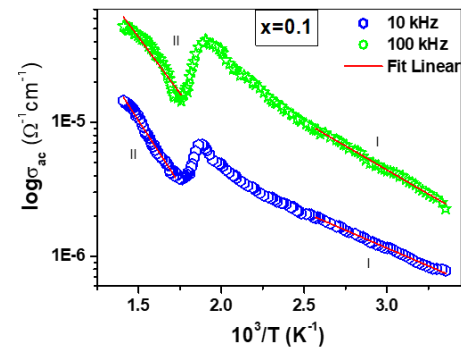


Fig. 5. Variation of σ_{ac} with $1000/T$ of $\text{Li}_{0.5}\text{Bi}_{0.5}\text{Ti}_{0.9}\text{Zr}_{0.1}\text{O}_3$ at two selected frequencies

Table 1
 Comparison of activation energy E_a (eV) of $\text{Li}_{0.5}\text{Bi}_{0.5}\text{Ti}_{0.9}\text{Zr}_{0.1}\text{O}_3$ at two different frequencies in region I and II, calculated from σ_{ac} vs. $1/T$ graphs

Frequency (kHz)	Activation energy E_a (eV)	
	Region I	Region II
10	0.1058	0.3790
100	0.1421	0.3317

D. Complex Impedance Spectroscopy

Complex impedance spectroscopy technique is an effective and simple flexible method to analyze the frequency dependent response of various electrical parameters and effects (grain, grain boundary and electrode effect etc.) of the compound in conjunction with simple impedance formulation. The output response in the studied specimen is measured by applying an ac signal across the sintered pellet. Fig. 6 indicates the frequency dependence of impedance plots at the selected temperatures. The decreasing nature of the real part of impedance (Z') with the increase in frequency and temperature can be indicated in the figure. In the high-frequency region, Z' coincides with each other to attain an approximately constant value. The complete merging of the curves of Z' for different temperatures at high frequencies (above 100 kHz) may be due to the semiconductor

Table 2
Resistance (R_g , R_{gb}) and capacitance (C_g , C_{gb}) of grains and grain boundaries of $\text{Li}_{0.5}\text{Bi}_{0.5}\text{Ti}_{0.9}\text{Zr}_{0.1}\text{O}_3$ ceramics

Temperature ($^{\circ}\text{C}$)	R_g (Ω)	R_{gb} (Ω)	C_g (F)	C_{gb} (F)
300	1.178E+007	3.234E+002	2.660E-020	9.930E-008
325	8.009E+006	7.297E+009	4.031E-011	5.261E+005
350	6.925E+006	3.827E-011	2.117E+004	5.030E-012
375	5.541E+006	1.000E-002	4.150E-011	6.567E-012
400	4.253E+006	1.228E+005	4.475E-011	4.759E-011
425	2.899E+006	9.132E+004	4.728E-011	4.153E-011

properties, and release of space charges. The declining trend of Z' value reveals the presence of negative temperature coefficient of resistance behaviour in the material [25].

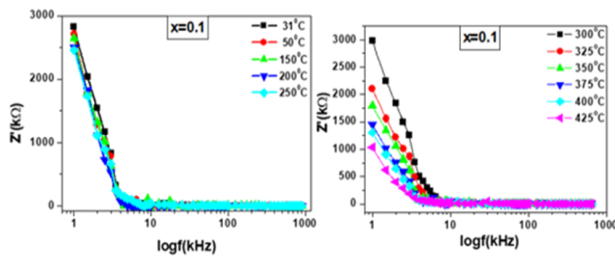


Fig. 6. $Z'' \sim \log f$ of $\text{Li}_{0.5}\text{Bi}_{0.5}\text{Ti}_{0.9}\text{Zr}_{0.1}\text{O}_3$ at various temperatures

Figure 7 (a and b) and figure 8 represents the variation of imaginary part of impedance (Z'') and modulus as a function of frequency at different temperatures for $\text{Li}_{0.5}\text{Bi}_{0.5}\text{Ti}_{0.9}\text{Zr}_{0.1}\text{O}_3$ ceramic. In the lower frequency side, normal variations in Z'' values with temperature and frequency were observed and all the curves at different temperatures appear to merge in to a single curve in the higher frequency region (figure 7 a & b). The variation of Z'' of the compound indicate that NTCR behavior is observed. The shifting of the Z''_{max} in the direction of high frequency side in high temperature region is a consequence of relaxation phenomenon in the system. The reduction in resistance of grain when temperature rises is the cause of the shifting of peaks. Merging of all these curves at fusion frequency (f_i) is a symptom of the gathering of space charge in the studied compounds [21]. The low frequency region peak corresponds to grain boundary, while higher frequency region peak represents the bulk (grain) contribution. Decrement in peak height of the impedance spectra with rise in temperature is a characteristic feature very familiar in polycrystalline ceramics [22-24] which indicates temperature evolutions of relaxation processes. The value of resistance and capacitance for grain and grain boundary were obtained using the relation $2\pi f_m R C = 1$ from Z'' vs $\log f$ plot and indicating contributions from grain and grain boundary in the samples. Appearance of nonexistence of Debye type relaxation process with variety of relaxation time is because of the contribution of bulk and bulk interface [38].

The figure 8 shows the plot of imaginary part M'' with frequency at different temperatures. The use of modulus spectroscopic plot is particularly useful for separating component with similar resistance but different capacitance. In figure 8, peaks appear to be shifted towards higher frequency side with rise in temperature. It is also observed that M'' peaks

broaden with decrease in temperature. The observed temperature and frequency dependence of M'' arises due to distribution of relaxation time in the sample. The broadening of M'' spectra must be intrinsically non-exponential process, like inter relationship among diffusion of the charged species, or diversities in the microstructure of the material, leading sequentially distribution of conduction of localized charged species in space and time to respond electrical effect.

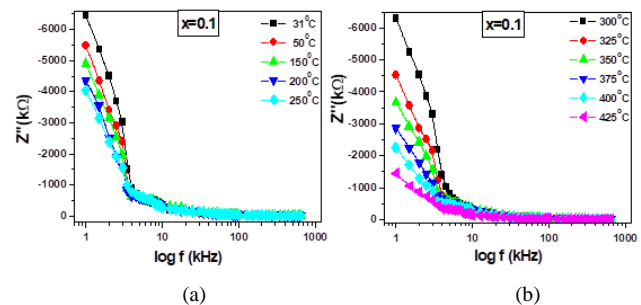


Fig. 7. (a) and (b): Frequency dependence of imaginary part of impedance Z'' at different temperatures for $\text{Li}_{0.5}\text{Bi}_{0.5}\text{Ti}_{0.9}\text{Zr}_{0.1}\text{O}_3$ ceramic sample

E. Nyquist plot

The Nyquist diagram (impedance spectrum) displays the variation of the real component of impedance (Z') with its imaginary (Z''). The impedance characteristics of the sample indicate the presence of bulk, grain boundaries and electrode interfaces effects in the material. With a rise in temperature, the impedance curves gradually bend to form semicircle (shown in inserted Fig. 9) with the change in their center point to the origin of the plot. This deviation in the pattern of the semicircular arc with variation in temperature suggests the impedance characteristic of the sample. Based on the analysis of the characteristics of the two semicircles formed in the temperature range of 31–425 $^{\circ}\text{C}$, we can conclude that the compound has both grain and grain boundary effects in the electrical properties. The values of grain resistance (R_g), grain boundary resistance (R_{gb}), grain capacitance (C_g) and grain boundary capacitance (C_{gb}) are shown in table 2.

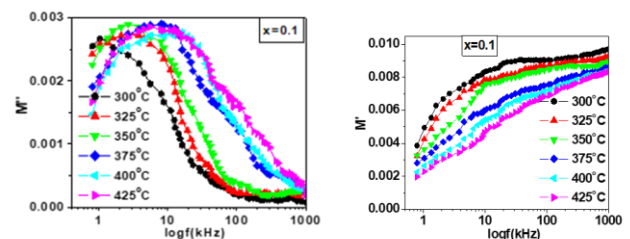


Fig. 8. Frequency dependence of real M' & imaginary part of modulus M'' at different temperatures for $\text{Li}_{0.5}\text{Bi}_{0.5}\text{Ti}_{0.9}\text{Zr}_{0.1}\text{O}_3$ ceramic sample

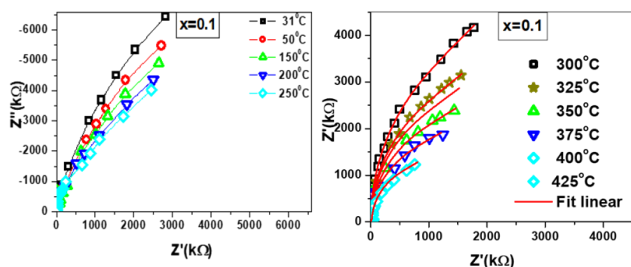


Fig. 9. Variation of Z' with Z'' at different temperature of $\text{Li}_{0.5}\text{Bi}_{0.5}\text{Ti}_{0.9}\text{Zr}_{0.1}\text{O}_3$

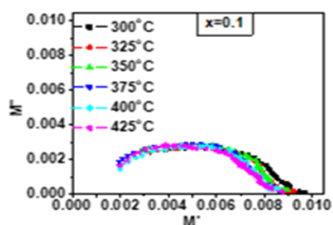


Fig. 10. Variation of M' with M'' at different temperature of $\text{Li}_{0.5}\text{Bi}_{0.5}\text{Ti}_{0.9}\text{Zr}_{0.1}\text{O}_3$

4. Conclusion

The polycrystalline sample of LBTZ was set up by a solid state-reaction route. Preliminary X-ray examination affirms the single phase orthorhombic crystal structure at room temperature. The plot solidly settled the ferro to paraelectric phase transition at 258°C . Addition of Zr increases room temperature and peak dielectric constant values, which can be useful for dielectric for capacitor application. The dielectric constant of the ceramics diminishes with increasing frequency. Impedance and modulus spectroscopy reveals the presence of grain and grain boundary contribution in the sample and complex impedance analysis targeted the relaxation phenomenon is poly disperse and non-Debye type in nature. The activation energy of the compound was found to be distinctive in various regions demonstrating presence of various conduction components.

Acknowledgement

D. Panda acknowledges North Orissa University for the co-operation and help during his Ph.D. research work. He extremely grateful to Director, PXE, Chandipur, for allowing him for the research programme. The authors are thankful to Prof. R. N. P. Choudhary, Professor, Department of Physics, ITER, Bhubaneswar who had helped us and permitted us to use his laboratory during synthesis of compound and some of analysis of its properties. D. Panda also acknowledges Department of Physics, Betnoti College Betnoti for allowing him to do some experimental work during his research.

References

[1] Y. Saito, H. Takao, T. Tani, T. Nonoyama, K. Takator, T. Homma, T.Nagaya, and M. Nakamura: Nature 432 (2004) 84.

[2] S. T. Zhang, A. B. Kounga, E. Aulbach, H. Ehrenberg, and J. Rödel: Appl. Phys. Lett. 91 (2007) 112906.

[3] T. Takenaka, H. Nagata, and Y. Hiruma: Jpn. J. Appl. Phys. 47 (2008) 3787.

[4] J.C. Anderson, Dielectrics, Chapman and Hall, London, 1964.

[5] S.K. Pradhan, S.N. Das, S. Halder, S. Bhuyan, R.N.P. Choudhary, J. Mater. Sci.: Mater. Electron. 28 (2007) 9627–9633.

[6] Zhu, X.L., Chen, X.M., Liu, X.Q. and Yuan, Y. (2006) Dielectric Characteristics and Diffuse Ferroelectric Phase Transition in $\text{Sr}_4\text{La}_2\text{Ti}_4\text{Nb}_6\text{O}_{30}$ Tungsten Bronze Ceramics. Journal of Materials Research, 21, 1787-1792.

[7] Huang, C., Bhalla, A.S. and Guo, R. (2005) Measurement of Microwave Electro-Optic Coefficient in $\text{Sr}_{0.61}\text{Ba}_{0.39}\text{Nb}_2\text{O}_6$ Crystal Fiber. Applied Physics Letters, 86.

[8] Ramirez, M.O., Jaque, D., Bausa, L.E., Sole Garci, J. and Kaminskii, A.A. (2005) Near Infrared and Visible Tunability from a Diode Pumped Nd Activated Strontium Barium Niobate Laser Crystal. Physical Review Letters, 95.

[9] Rao, K.S. and Nath, N.V. (2005) Influence of Rare-Earth Ion on Piezoelectric and Pyroelectric Properties of PBN System. Ferroelectrics, 325, 15-24.

[10] Jiang, W., Cao, W., Yi, X. and Chen, H. (2005) The Elastic and Piezoelectric Properties of Tungsten Bronze Ferroelectric Crystals ($\text{Sr}_{0.7}\text{Ba}_{0.3}$) $_2\text{NaNb}_5\text{O}_{15}$ and ($\text{Sr}_{0.3}\text{Ba}_{0.7}$) $_2\text{NaNb}_5\text{O}_{15}$. Journal of Applied Physics, 97.

[11] Raju, M.R. and Choudhary, R.N.P. (2006) Effect of Zr Substitution on Structural, Dielectric and Electrical Properties of $\text{Sr}_5\text{SmTi}_3\text{Nb}_7\text{O}_{30}$ Ceramics. Materials Chemistry and Physics, 99, 135-143.

[12] Chen, W., Kinemuchi, Y., Watari, K., Tamura, T. and Miwa, K. (2006) Preparation of Grain-Oriented $\text{Sr}_{0.5}\text{Ba}_{0.5}\text{Nb}_2\text{O}_6$ Ferroelectric Ceramics by Magnetic Alignment. Journal of the American Ceramic Society, 89, 381-384.

[13] Ko, H., Kojima, S., Lushnikov, S.G., Katiyar, R.S., Kim, T.-H. and Ro, J.-H. (2002) Low-Temperature Transverse Dielectric and Pyroelectric Anomalies of Uniaxial Tungsten Bronze Crystals. Journal of Applied Physics, 92, 1536. <https://doi.org/10.1063/1.1491995>

[14] Wu, E. (1989) POWD, an Interactive Powder Diffraction Data Interpretation and Index Program. Ver.2.1. School of Physical Science, Flinders University South Bedford Park, Australia.

[15] Geiss, E.A., Scott, B.A., Burns, G., O’Kane, D.F. and Segmuller, A. (1969) Alkali Strontium-Barium-Lead Niobate Systems with a Tungsten Bronze Structure: Crystallographic Properties and Curie Points. Journal of the American Ceramic Society, 52, 276-281.

[16] Klug, H.P. and Alexander, L.E. (1974) X-Ray Diffraction Procedures for Polycrystalline and Amorphous Materials. Wiley-Interscience, New York.

[17] Sahho, P.S., Panigrahi, A., Patri, S.K. and Choudhary, R.N.P. (2010) Impedance Spectroscopy of $\text{Ba}_3\text{Sr}_2\text{DyTi}_3\text{V}_7\text{O}_{30}$ Ceramic. Bulletin of Materials Science, 33,129-134.

[18] Dash, S., Choudhary, R.N.P. and Kumar, A. (2014) Impedance Spectroscopy and Conduction Mechanism of Multiferroic ($\text{Bi}_{0.6}\text{K}_{0.4}$)($\text{Fe}_{0.6}\text{Nb}_{0.4}$) O_3 . Journal of Physics and Chemistry of Solids, 75, 1376-1382.

[19] Singh, A.K., Barik, S.K., Choudhary, R.N.P. and Mahapatra, P.K. (2009) Ac Conductivity and Relaxation Mechanism in $\text{Ba}_{0.9}\text{Sr}_{0.1}\text{TiO}_3$. Journal of Alloys and Compounds, 479, 39-42.

[20] Bhattacharya, S., Bharadwaj, S.S.N. and Krupanidhi, S.B. (2000) Alternating Current Conduction Behavior of Excimer Laser Ablated $\text{SrBi}_2\text{Nb}_2\text{O}_9$ Thin Films. Journal of Applied Physics, 88, 4294.

[21] P. S. Sahoo, A. Panigrahi, S.K. Patri, R. N. P. Choudhary, Bull. Metr. Sc. 33 (2) (2010) 129.

[22] S. Saha, T.P. Sinha, Phys. Rev. B 65 (2002)134103.

[23] S. Sen, P. P. Ramanik, R. N. P. Choudhary, Appl. Phys. A82(2006) 549

[24] Y. Hosono, K. Harada, Y. Yamashita, Jpn. J. Appl. Phys. 40 (2001), 5722.

[25] D.C. Sinclair, A.R. West, “Impedance and modulus spectroscopy of semiconducting BaTiO_3 showing positive temperature coefficient of resistance”, J. Appl. Phys., 66 (1989) 3850.

[26] S. Sahoo, P. K. Mahapatra, R. N. P. Choudhary, “The structural, electrical and magnetoelectric properties of softchemically-synthesized SmFeO_3 ceramics”, J. Phys. D: Appl. Phys., 49 (2016) 035302.

- [27] S.K. Dehury, K. Parida, R.N.P. Choudhary, "Dielectric, impedance and magneto-electric characteristics of $\text{Bi}_{0.5}\text{Sr}_{0.5}\text{Fe}_{0.5}\text{Ce}_{0.5}\text{O}_3$ electronic material", *J. Mater. Sci.: Mater. Electron.*, 28 (2017) 10441–10448.
- [28] B. Garbarz-Glos, W. B. ak, M. Antonova, M. Pawlik, "Structural, microstructural and impedance spectroscopy study of functional ferroelectric ceramic materials based on barium titanate", *IOP Conf. Ser.: Mater. Sci. Eng.*, 49 (2013) 012031.
- [29] B.E. Vugmeister, M.D. Glinichuk, "Dipole glass and ferroelectricity in random-site electric dipole systems", *Rev.Mod. Phys.*, 62 (1990) 993–1026.
- [30] R. Ranjan, R. Kumar, N. Kumar, B. Behera, R. N. P. Choudhary, "Impedance and electric modulus analysis of Sm-modified $\text{Pb}(\text{Zr}_{0.55}\text{Ti}_{0.45})_{1-x}/\text{O}_3$ ceramics", *J. Alloys Compd.*, 509 (2011) 6388–6394.
- [31] A. Rouahi, A. Kahouli, F. Challali, M.P. Besland, C. Vallée, B. Yangui, S. Salimy, A. Goullet, A. Sylvestre, "Impedance and electric modulus study of amorphous TiTaO thin films: Highlight of the interphase effect", *J. Phys. D: Appl. Phys.*, 46 (2013) 065308.
- [32] M. Idrees, M. Nadeem, M.M. Hassan, "Investigation of conduction and relaxation in MoS_2 nanoflakes synthesized by simple solid state reaction", *J. Appl. Phys.*, 113 [4] (2013) 043704–043706.
- [33] Xiao, S.X. and Yan, X.P. (2009) Preparation and Characterization of Si-Doped Barium Titanate Nanopowders and Ceramics. *Micro electronic Engineering*, 86, 387-391.
- [34] Rath, M.K., Pradhan, G.K., Pandey, B., Verma, H.C., Roul, B.K. and Anand, S. (2008) Synthesis, Characterization and Dielectric Properties of Europium-Doped Barium Titanate Nanopowders. *Materials Letters*, 62, 2136-2139.
- [35] Gulwade, D. and Gopalan, P. (2008) Diffuse Phase Transition in La and Ga Doped Barium Titanate. *Solid State Communications*, 146, 340-344.
- [36] Unruan, M., Sareein, T., Tangsittrakul, J., Prasertpalichatr, S., Ngamjarurojana, A., Anata, S. and Yimnirun, R. (2008) Changes in Dielectric and Ferroelectric Properties of $\text{Fe}^{3+}/\text{Nb}^{5+}$ Hybrid-Doped Barium Titanate Ceramics under Compressive Stress. *Journal of Applied Physics*, 104.
- [37] Yaseen, H., Baltianski, S. and Tsur, Y. (2006) Effect of Incorporating Method of Niobium on the Properties of Doped Barium Titanate Ceramics. *Journal of the American Ceramic Society*, 89, 1584-1589.
- [38] Cha, S.H. and Han, Y.H. (2006) Effects of Mn Doping on Dielectric Properties of Mg-Doped BaTiO_3 . *Journal of Applied Physics*, 100, Article ID: 104102.
- [39] Shen, Z.J., Chen, W.P., Qi, J.Q., Wang, Y., Chan, H.L.W., Chen, Y. and Jiang, X.P. (2009) Dielectric Properties of Barium Titanate Ceramics Modified by SiO_2 and by BaO-SiO_2 . *Physica B: Condensed Matter*, 404, 2374-2376.
- [40] Kirianov, A., Hagiwara, T., Kishi, H. and Ohsato, H. (2002) Effect of Ho/Mg Ratio on Formation of Core-Shell Structure in BaTiO_3 and on Dielectric Properties of BaTiO_3 Ceramics. *Japanese Journal of Applied Physics*, 41, 6934-6937.
- [41] Wang, S., Zhang, S.R., Zhou, X.H., Li, B. and Chen, Z. (2005) Effect of Sintering Atmospheres on the Microstructure and Dielectric Properties of Yb/Mg Co-Doped BaTiO_3 Ceramics. *Materials Letters*, 59, 2457-2460.
- [42] Rout, S.K., Sinha, E. and Panigrahi, S. (2007) Dielectric Properties and Diffuse Phase Transition in $\text{Ba}_{1-x}\text{Mg}_x\text{Ti}_{0.6}\text{Zr}_{0.4}\text{O}_3$ Solid Solutions. *Materials Chemistry and Physics*, 101, 428-432.
- [43] Henning, D., Schnell, A. and Simon, G. (1982) Diffuse Ferroelectric Phase Transitions in $\text{Ba}(\text{Ti}_{1-y}\text{Zr}_y)\text{O}_3$ Ceramics. *Journal of the American Ceramic Society*, 65, 539-544.
- [44] Yu, Z., Guo, R. and Bhalla, A.S. (2000) Dielectric Behavior of $\text{Ba}(\text{Ti}_{1-x}\text{Zr}_x)\text{O}_3$ Single Crystals. *Journal of Applied Physics*, 88, 410.